Proceedings of the 11th ICPMG 2026
11th International Conference on Physical Modelling in Geotechnics
8-12 June 2026, Zurich, Switzerland

Installation and inclined loading response of drag embedment anchors in sand and clay

D. A. Dao
Hamburg University of Technology, Hamburg, Germany, duy.anh.dao@tuhh.de

A. Peccin da Silva, D. A. de Lange, S. J. M. van Eekelen
Deltares, Delft, Netherlands, anderson.peccindasilva@deltares.nl, dirk.delange@deltares.nl
suzanne.vaneekelen@deltares.nl,

ABSTRACT: Drag embedment anchors (DEAs) secure floating offshore structures by embedding into the seabed and offer high potential for upscaling, particularly in deeper offshore regions. However, the anchor load-displacement response is not fully understood. This study presents a series of centrifuge tests to model the installation and inclined loading behaviour of DEAs under an acceleration level of 100*g*. Steel-printed DEA models with fluke-shank angles of 32 and 45° were embedded into sand and clay samples by pulling the mooring line during centrifuge spinning, followed by unidirectional further inclined pulling. Pull loads were recorded continuously. Post-testing procedures included dissecting soil samples and conducting 3D scans, allowing approximations of the anchor trajectory. Results indicate that once the anchor reaches its maximum penetration depth, it stays in equilibrium provided that changes in the mooring line angle and the resulting vertical load component remain small so that motion is predominantly horizontal. Therefore, care must be taken when higher angles are considered in design. Moreover, consistent force-displacement profiles show that anchor force depends primarily on penetration depth rather than drag distance.

1 INTRODUCTION

The stability and safety of floating structures rely significantly on the performance of mooring systems, with anchors, such as the drag embedment anchor (DEA), playing a crucial role in ensuring station-keeping. As demand for floating facilities grows, the required number and efficiency of anchors are also expected to increase (Cerfontaine et al., 2023; Gourvenec, 2024). However, improving the efficiency of DEA design requires a better understanding of the interactions between the anchors and the seabed under varying load conditions. Although most existing studies focus on anchor chain integrity, limited attention has been given to the critical soil-anchor interactions that are essential for the overall safety of floating systems (Hong et al., 2024). Previous centrifuge tests, such as those by Neubecker and Randolph (1996a) and Neubecker and Randolph (1996b), have proposed a three-dimensional soil wedge model for predicting holding capacity. Davidson et al. (2023) explored DEA performance under out-of-plane loading. Fan et al. (2026) and Davidson et al. (2023); Sharif et al. (2025a,b) presented improved methods for accurately determining the position of DEAs during centrifuge testing, enabling more precise analyses of anchor kinematics. Fewer laboratory studies investigated embedment kinematics in clay (O'Neill and Randolph, 2001; O'Neill et al., 2003; Chen et al., 2023) and performance in layered clay profiles (Lai et al., 2020) under monotonic loading. For both sand and clay, the effects of sequential loading on anchor behaviour have not yet been systematically investigated.

Moreover, to reduce the spatial footprint of long mooring lines, one possible approach is to apply an inclined load to the anchor instead of a purely horizontal load at the seabed. While Sharif et al. (2025a) conducted centrifuge tests in which anchors were pulled at constant inclination angles of 10 and 20° in sand, available data on the inclined loading response of DEAs in clay remain limited. API RP 2SK (2024) provides data for anchors in soft clay under loading angles up to 20°. However, stiffer clays and larger inclined loading angles have not yet been investigated.

This study presents the results of centrifuge tests modelling the anchor installation and analysing the effects of sinusoidal loading under an acceleration level of 100*g* (Dao et al., 2024, 2025). Furthermore, inclined loading was applied to identify the conditions under which the anchor line angle affects anchor stability.

2 TESTING PROGRAM

This study was conducted at the geotechnical Actidyn C72-3 beam centrifuge of Deltares, Delft, Netherlands. The centrifuge has a platform radius of 5 m and was operated at 100*g*, defined at the soil surface, for the presented tests. The program included seven anchor tests across four different soil samples, varying in soil composition and loading conditions. The testing procedure involved placing the DEA on a platform above the mudline, embedding it by pulling the anchor's mooring line, and applying a sinusoidal loading, and pulling it out. Tension/compression load cells with a nominal capacity of 20 kN measured the pull force corresponding to the prescribed actuator displacement. When two anchors were installed in the same container, the corresponding tests were performed sequentially during the same centrifuge flight. After each test, the anchor remained in the container. For the sand tests, dye was applied in a layer to the soil sample during preparation to facilitate tracking the anchor's movement over time retrospectively. The sample was dissected to locate coloured or void traces left by the fluke tip. The coordinates of the traces were measured from 3D scans of the dissected cross-sections in the point-cloud software CloudCompare to approximate the trajectory of the anchor. Table 1 outlines the conducted tests with varying loading sequences, detailed in Section 5.

3 ANCHOR MODELS

A 1:100 scaled DEA roughly based on a 10 t Stevshark Rex was used, as presented in Figure 1. The model's minimum thickness of 0.7 mm exceeded the thickness of the reference anchor when scaled to prototype dimensions. Two stainless steel 3D printed models of the anchor were used in the centrifuge tests, measuring 55 mm in fluke width w_f, 28/35 mm in anchor height h_a for sand and clay and 35 mm in fluke length L_f with a mass of 20 g. The configuration of the fluke-shank angle could be switched between of 32 and 45°. Each soil sample underwent up to two anchor tests. Commercially available 12-strand braided Dyneema ropes with a nominal diameter of 3 mm were used as mooring lines.

4 SOIL SAMPLES

In total, four soil samples were produced. Table 2 and Table 3 summarise the index properties of the two used soils. Each soil sample was prepared in a container with measurements according to Figure 2.

Table 1. Test matrix with loading sequences: s1, s2, p (Pull), s3

ID	Soil Model	Phase I	Phase II	Phase III
1a	1 (sand)	Installation	–	Pullout
1b	1 (sand)	Installation	s1	Pullout
2a	2 (sand)	Installation	s2, p, s2, p, s2, p, s2	Pullout
2b	2 (sand)	Installation	s3, p, s3, p, s3, p, s3	Pullout
3a	3 (clay)	Installation	–	Pullout
3b	3 (clay)	Installation	s1	Pullout
4	4 (clay)	Installation	s3	Pullout

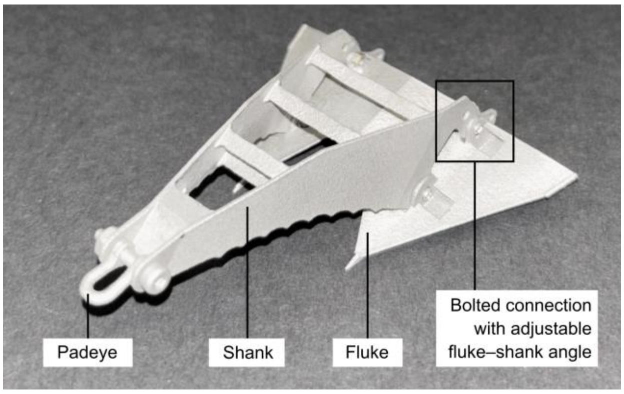

Figure 1. 3D printed anchor model

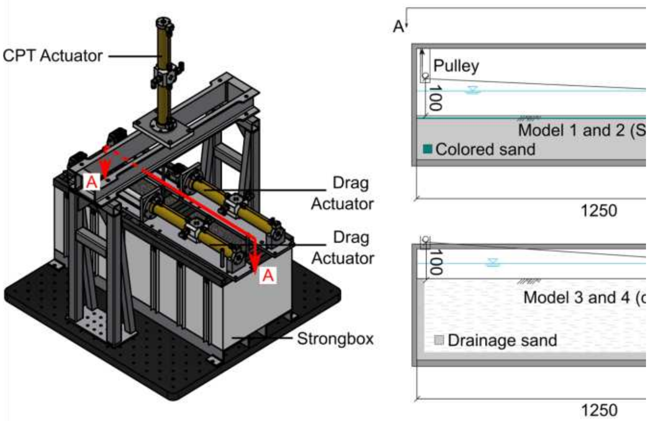

Figure 2. Setup inside the centrifuge and setup of the strongbox for clay and sand tests

The coarse-grained soil used for Sample 1 and 2 is Baskarp B15 sand, which is classified as a poorly graded sand. The dry sand was pluviated into a water-filled test box, interspersed with a coloured sand layer. Soil layers were dyed according to de Lange and Langstraat (2024) and were placed at the expected minimum penetration depths of 10 mm from the mudline to facilitate post-test trajectory reconstruction.

CPTs were conducted during centrifuge spinning prior to anchor dragging to characterise the sand properties, see Figure 3. Based on the CPT correlation proposed by Jamiolkowski et al. (2003), both samples exhibit a relative density of about 30% at a depth of 2.5 m (model scale: 25 mm), corresponding to loose sand. This density range is representative of typical offshore sand deposits (Randolph and Gourvenec, 2011). Although the CPT results differ considerably beyond a depth of 7 m (model scale: 70 mm), they remain comparable above this depth. Since the maximum penetration depth of the anchor was within this range ($0.7L_f$ = 2.31 m, model scale: 23.1 mm), the two soil samples are considered to be sufficiently similar in the relevant anchor-soil interaction zone.

The kaolin slurry was prepared at a water content equal to 2.5 times the liquid limit and preconsolidated at 285 kPa. CPTs were performed at 100*g*. The undrained shear strength (s_u) was derived from the corrected cone tip resistance (q_t) using the standard empirical relationship (Lunne et al., 2002) $s_u = (q_t - \sigma_v)/N_{kt}$, where σ_v is the total vertical stress, and N_{kt} is the cone factor, set to be 18. Figure 4 shows the undrained shear strength profile which increased approximately linearly with depth. The shear strength between 0 and 10 m (model scale: 100 mm) was classified as medium stiff clay, and strength below 10 m (model scale: 100 mm) as stiff clay, following ASTM D2488 (2018) and BS 8004:2015 (2015). The peak values of the undrained shear strength that the anchor models reached in Samples 3 and 4 were 46.8 kPa and 64.3 kPa, respectively.

5 ANCHOR LOADING

During the tests, a hydraulic cylinder applied a unidirectional pulling load on the mooring line. A drag anchor test included three distinct phases. The drag velocities were chosen so that the dimensionless velocity $V = vL_f/c_v = 2.7 \times 10^5$ for the clay tests, as proposed by Finnie and Randolph (1994), where v is the drag velocity, L_f the fluke length, and c_v the vertical coefficient of consolidation, exceeded the minimum limits reported by Finnie and Randolph (1994), House et al. (2001), Chung et al. (2006), and Cassidy (2012), i.e., of at least 30 for undrained conditions in the clay tests. For the sand tests, with an assumed $c_v \approx 10^{-3}$ m^2/s, V is well below 1, representing drained conditions (Randolph and Gourvenec, 2011).

Phase I (Installation): The DEA was initially positioned on a plate and then pulled at a speed of 1 mm/s to embed it into the soil at 100*g*. The installation continued by dragging the anchor at a speed of 10 mm/s, achieving a minimum drag path of 32 m (model scale: 320 mm) in sand and 80 m (model scale: 800 mm) in clay.

Phase II (Loading):

- Sinusoidal Loading: Loads were transformed from force-controlled $F(t)$ to displacement-controlled $x(t)$ inputs using a linear mapping. This function was derived from calibration tests that measured the force-displacement relation-ship with a load cell. Load ranges for these scenarios were determined using the panel code panMare by Schulz et al. (2022). After a reduction of the force at the end of Phase I by 60%, the converted displacement time series, as presented in Figure 5, were applied. For the smallest loading amplitudes and frequencies, V is approximately 50, which exceeds the threshold value of 30 for undrained conditions in clay. For the sand tests, the resulting V remain below unity, indicating drained conditions during Phase II.
- Pull: In tests 2a and 2b, after sinusoidal loading, the anchor underwent a pulling phase at a speed of 10 mm/s for 15 s before the next sinusoidal loading.

Phase III (Pull-Out): Following the first two phases, the anchor was pulled continuously at 1 mm/s until it reached the end of the test box.

Table 2. Baskarp sand properties

Parameter	Value
Specific gravity, G_s	2.65
Median particle diameter, d_{50} (mm)	0.136
Coefficient of uniformity, C_u	1.4
Minimum void ratio, e_{min}	0.549
Maximum void ratio, e_{max}	0.858
Friction angle φ (°)	30.1

Table 3. Kaolin clay properties

Parameter	Value
Specific gravity, G_s	2.63

Median particle diameter, d_{50} (mm)	0.0076
Liquid limit, LL (%)	59.9
Plastic limit, PL (%)	31.2
Slope of normal consolidation line, λ	0.276
Slope of swelling line, κ	0.048
Coefficient of vertical consolidation, c_v (m^2/s) (at OCR = 1 and σ'_v = 30 kPa)	1.3×10^{-7}

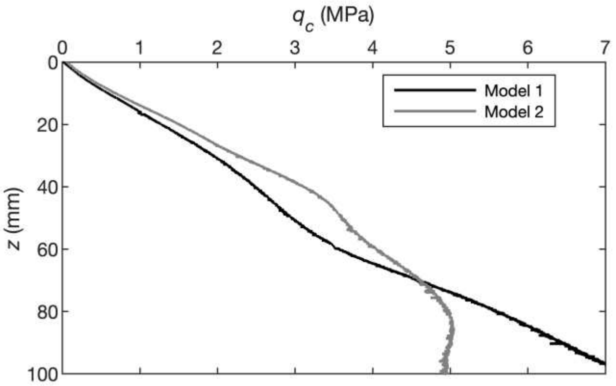

Figure 3. CPT results of the sand models

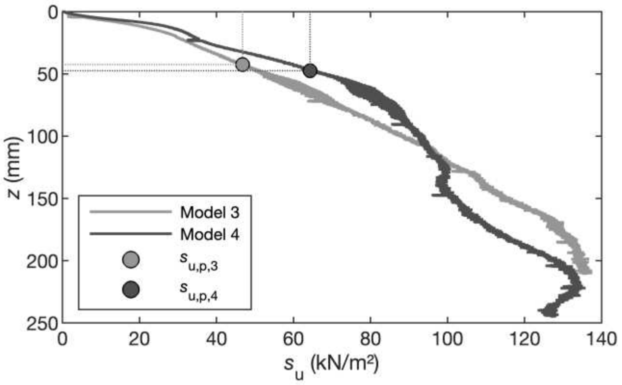

Figure 4. Undrained shear strength profile derived from CPT for the clay models

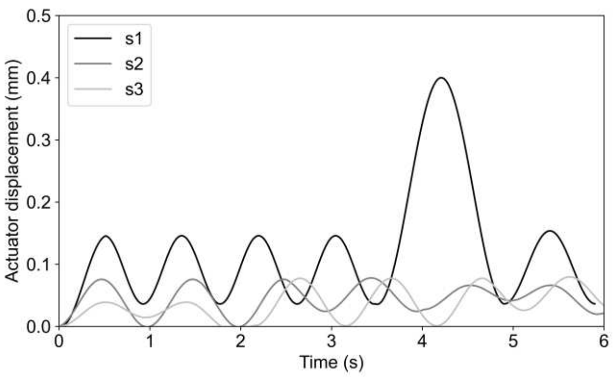

Figure 5. Phase II loading cases

6 MEASURING POST TESTING

Figure 6 presents the procedure of taking measurements after testing. The soil sample was drained and sectioned at approximately regular intervals. 3D surface scans were taken after dissectioning using an EinScan HX handheld scanner. The procedure yielded a coloured 3D mesh aligned with the test axes, which were imported into CloudCompare for digital depth measurements of the scanned surface. For sand, the deformation field was inferred from the disturbance of the coloured layer. Zones of densification and loosening around the anchor fluke tips were highlighted effectively. Identifying changes in colour during dissecting enabled the estimation of fluke tip penetration depth. The depth at which these changes ceased (z-coordinate) was used to determine the deepest point reached by the anchor at specific horizontal positions (x and y coordinates). For the clay tests, impressions of the entire anchor as well as void traces of the fluke tips were identifiable.

7 RESULTS AND DISCUSSION

The plots, showing various parameters as functions of either the anchor line angle or the horizontal displacement, were divided into ranges representing distinct kinematic patterns regarding penetration behaviour. The three stages included: (1) embedment, in which the penetration depth increased up to (2) a quasi-steady stabilisation stage, in which penetration remained nearly constant, and (3) resurfacing, during which the penetration depth decreased due to pull-out. The division was performed separately for sand and clay tests, based on the penetration-displacement behaviour shown in Figure 7 and Figure 12.

The horizontal anchor line displacement was approximated from the actuator displacement using the relation $d_h \approx 4d_{actuator}$. This relation was verified by measuring the total drag path and comparing it with the recorded actuator displacement.

Both the anchor line inclination α and the pull angle increase with towing distance. The anchor line inclination α was approximated by

$$\alpha \approx \arctan\left(\frac{z_0+d_p-h_A}{x_0-d_p}\right) \quad (1)$$

Figure 6. Measurement procedure after testing: dissecting soil samples, scanning soil surfaces, and analysis of 3D scan

where z_0 denotes the vertical distance between the pulley and the mudline, d_p is the fluke penetration, h_A is the anchor height, and x_0 is the horizontal distance from the pulley to the initial seabed contact point.

The measured forces were normalised using theoretical holding capacities derived from Neubecker and Randolph (1996b) for sand and from O'Neill et al. (2003) for clay.

Overall, no significant change in the load-displacement behaviour of the anchors due to the loading sequence of Phase II was observed, suggesting that the anchors remained safe under the applied sinusoidal loads. However, possible changes in stiffness could not be captured with the available instrumentation. Detecting such effects will require more accurate position measurement techniques, such as photogrammetry (Fan et al., 2026) or the use of accelerometers (Davidson et al., 2023; Sharif et al., 2025a,b). Therefore, the influence of the loading sequence is not discussed in further detail.

To assess the accuracy of the approximation, we use the mean absolute percentage error (MAPE). For each observation, we take the absolute difference between the predicted and measured values, express it as a percentage of the measured value, and then average these percentages across all observations. The result is reported in percent. 0% denotes a perfect match.

7.1 Sand tests

Figure 7 shows the vertical anchor fluke tip position over the horizontal displacement, presenting typical penetration curves for anchors during installation and reaching ultimate holding capacity (UHC). The installation was carried out up to the drag distance of 32 m (d_h/L_f = 9.1, 320 mm in model scale), recommended by Delmar (2018) for sand. The anchor reached the UHC and thus the stabilisation stage considerably earlier. Below a normalised displacement of d_h/L_f = 5, the test results show only minor differences in penetration depth. However, these small deviations appear sufficient to cause pronounced variations beyond this point, even though the resulting anchor line angles during inclined loading were similar across all four sand tests and the CPT results indicated comparable relative densities for the space of interest.

Figure 8 shows the anchor line angle increasing approximately linearly up to a normalised horizontal displacement of about 17.5 and then growing more rapidly up to 15 and 19°. Figure 8 displays the resultant anchor force and its decomposition into horizontal and vertical components. The total and horizontal forces rise steeply to a stable level and then decrease gradually, whereas the vertical force decreases immediately after reaching its peak. This corresponds to the inflection point of α, where it begins to become larger at a higher rate.

The stabilisation phase, beginning at approximately d_h/L_f = 7.5, is characterised by an almost constant load and penetration depth over a considerable displacement range. Overall, the results presented in Figure 9 show a plausible trend, with an increasing force required for deeper penetration and a corresponding reduction in force during the extraction of the anchor. Differences in the magnitude of anchor force relative to anchor displacement are likely attributed to inherent heterogeneities within the soil sample, yet the overall trajectory of the force-displacement curves is similar.

The development of the load with respect to the anchor line angle, as shown in Figure 10, indicates that at an angle of approximately 9°, the inclination decreases anchor resistance and resurfacing is facilitated. These observations are consistent with the results reported by Sharif et al. (2025a), where reductions in UHC of 26.5% and 48% were observed for inclination angles of 10 and 20°, compared to purely horizontal loading. When comparing the UHC reduction of this study to Sharif et al. (2025a), the difference lies in 17.9% for 10°, showing similar loss in resistance.

Figure 11 shows the anchor force plotted against penetration depth. The colour brightness corresponds to the dragging distance, showing an increase in force with deeper penetration until the deepest point has been reached. Subsequently, as the anchor was pulled further, it began to resurface, leading to a decrease in the force required to pull the anchor.

Since the deeper of the two measured fluke depths was consistently used also in cases of possible rolling, this led to inconsistencies in the force-penetration relationship, particularly in Test 1a. Towards the end of the test, during resurfacing, lower forces were associated with larger penetration depths. Therefore, data points near the end of the horizontal drag phase were treated as outliers in subsequent analyses. The results suggest that the anchor force as a function of penetration depth $F(d_p)$ is unaffected by whether the anchor is in the embedment or in the resurfacing stage.

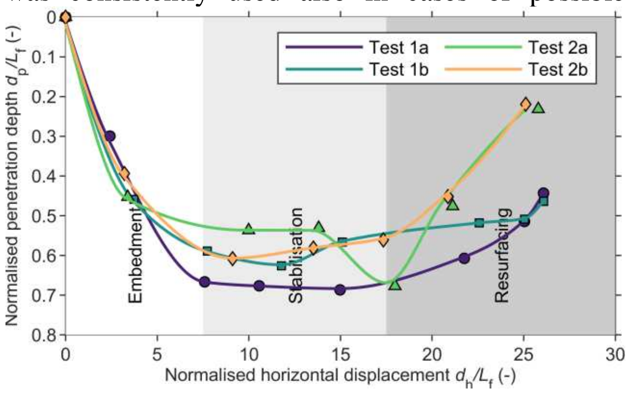

Figure 7: Anchor fluke penetration over horizontal displacement

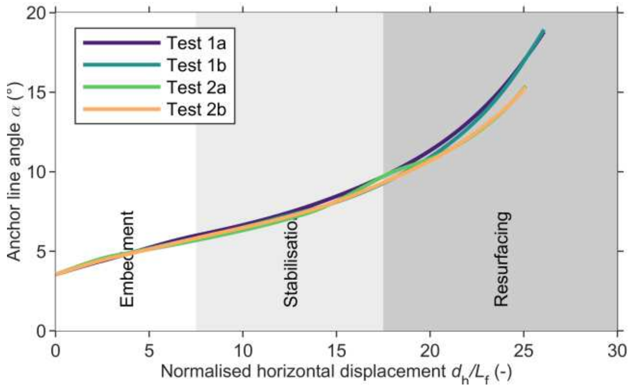

Figure 8: Anchor line angle at padeye over horizontal anchor displacement

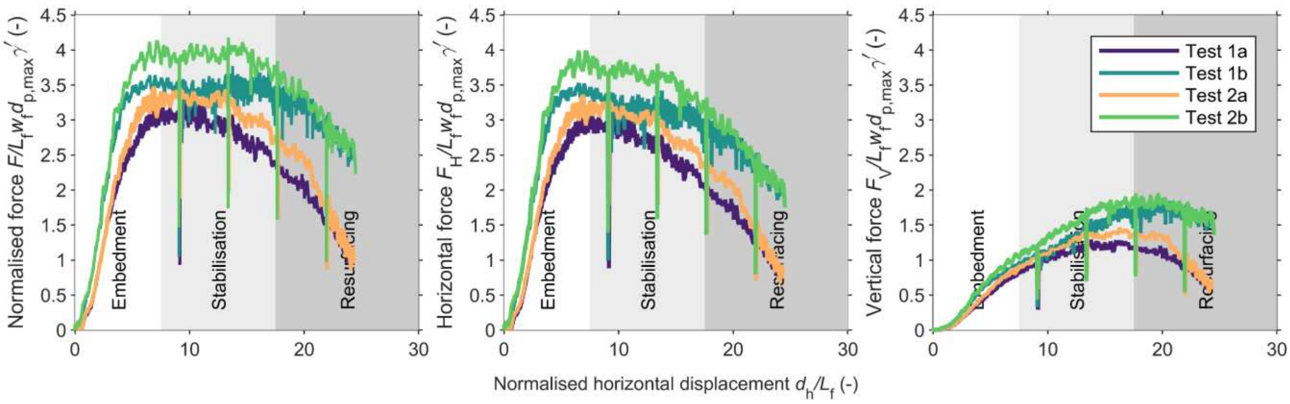

Figure 9: Pulling force over horizontal anchor displacement in sand tests

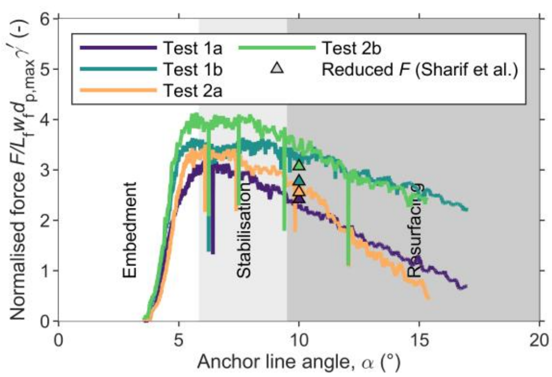

Figure 10. Pulling force over anchor line angle in sand

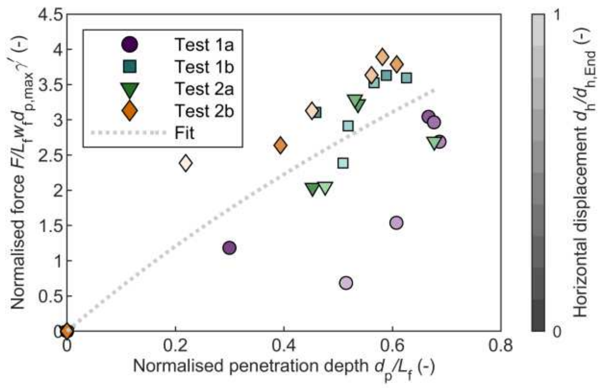

Figure 11. Pulling force over fluke penetration

7.2 Clay tests

Figure 12 presents the fluke penetration d_p as a function of the horizontal displacement. The three stages are also clearly distinguishable in the clay tests. However, stabilisation and resurfacing occur later, at approximately d_h/L_f = 13 and 21.5. Figure 13 also shows that destabilisation and resurfacing starts with higher anchor line angles. The later onset of the stages is consistent with the experience from manufacturers, who also recommend higher drag distances for their anchors in clay.

Regarding penetration, all three clay tests show the same trend during installation. After installation, a five minute pause, corresponding to a dimensionless time of $T = c_v t/L_f^2 = 0.032$, was introduced to allow for set-up effects. After this consolidation phase, Test 3a exhibited an earlier and larger loss of penetration depth than the other tests. Tests 3b and 4b behaved similarly during the quasi-steady stage. During resurfacing, the penetration depth responses diverged, but reached a similar final penetration depth, indicating a potential self-readjustment at high anchor line angles.

The three tests displayed similar patterns of force development in Figure 14 with different peak values as the drag distance increased and the line angle varied. Test 3a and 4 showed a lower anchor force, even before the Phase II sinusoidal load application began. The subsequent reduction in force is therefore more likely to be attributed to limited embedment, rather than to load-induced stiffness changes.

Compared to sand, the anchor in clay, as shown in Figure 15, becomes unstable at a higher angle of approximately 14° and exhibits a smaller reduction in load with increasing, even rapidly increasing, anchor line angle. The UHC reduction of DEAs in medium stiff clays aligns well with API RP 2SK (2024) values for soft clays with a difference of 9.7%.

The measured loads as a function of penetration depth, presented in Figure 16, follow the same general trend as observed for the anchor behaviour in sand. The results indicate that penetration depth is more relevant than drag distance, implying that the load-depth relationship remains consistent regardless of whether the anchor is in the embedment or resurfacing stage.

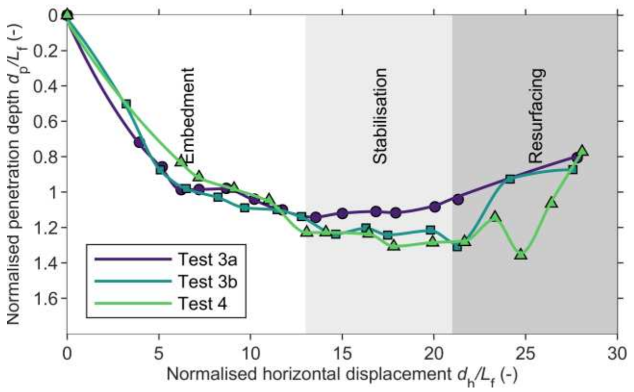

Figure 12. Anchor fluke penetration over horizontal displacement

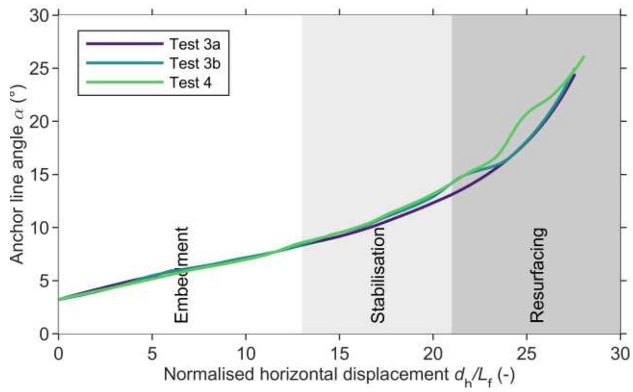

Figure 13. Anchor line angle at padeye over horizontal anchor displacement

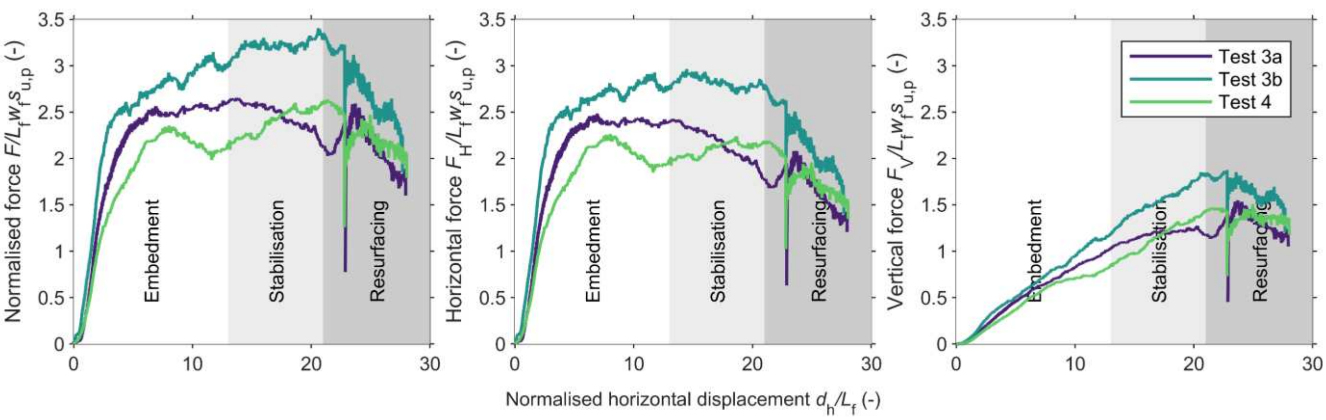

Figure 14. Pulling force over horizontal anchor displacement in clay

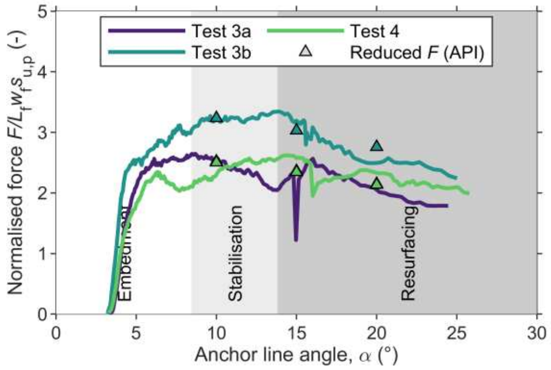

Figure 15. Pulling force over anchor line angle in clay

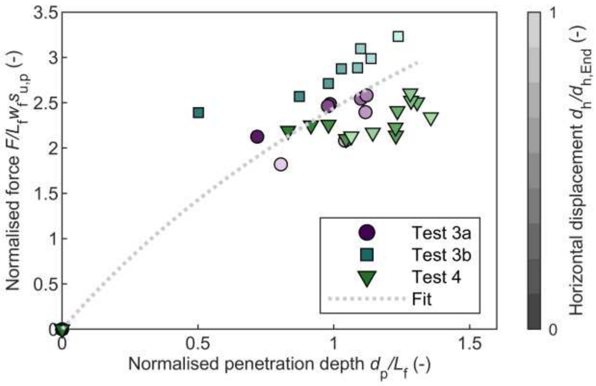

Figure 16. Pulling force over penetration depth

8 CONCLUSIONS

Seven centrifuge tests were conducted to model the installation and inclined loading behaviour of DEAs in sand and clay under an acceleration level of 100*g*. Each test comprised three phases: (I) installation, (II) sinusoidal loading, and (III) pull-out. The details of Phase II varied between tests; however, with the available instrumentation, a clear sensitivity of the displacement response to the specific loading sequence applied during this phase could not be identified.

The procedure introduced for dissecting and 3D scanning the soil samples enabled meaningful digital approximations of the anchor trajectory along the drag path. Nevertheless, detecting potential sequence effects on stiffness would require a more detailed position-tracking approach with a measurement precision on the order of 0.1 mm.

The measured anchor loads throughout the tests correlated primarily with the penetration depth and the anchor line angle. It was observed that the inclination influences anchor resistance, which decreases with increasing angle, thereby facilitating resurfacing. This trend is consistent with findings from previous studies, suggesting that care must be taken when higher angles are considered in design. Compared to sand, DEAs in clay are less affected by the change in anchor line angle.

Furthermore, critical anchor line angles were identified at which the anchor departs from equilibrium, resulting in a significant increase in the vertical load component and a corresponding reduction in overall resistance.

ACKNOWLEDGEMENTS

This project was supported by the Horizon 2020 research program of the European Union within the framework of the GEOLAB project, grant number 101006512, and by the German Research Foundation (Deutsche Forschungsgemeinschaft - DFG) under the funding code GR1024/61-1. We thank John Langstraat, Yao Su, Koen Castelein, Dirk Luger and Rob Zwaan from Deltares for their assistance in planning and carrying out the centrifuge tests. We extend our gratitude to the GEOLAB project partners, Eirini Papapanagiotou from Delmar, and Evelyn Heins from Grundbauingenieure Steinfeld und Partner Beratende Ingenieure mbB, as well as to Victor Remmers from Delmar and Jan Dührkop from Ramboll for their invaluable contributions. We would also like to thank our students, Andrew James Morrison and Katherine Nguyen, for their assistance in conducting and analysing the experiments.

REFERENCES

Cerfontaine B, White D, Kwa K, Gourvenec S, Knappett J and Brown M (2023) Anchor geotechnics for floating offshore wind: Current technologies and future innovations. *Ocean Engineering*, 279: 114327. http://doi.org/10.1016/j.oceaneng.2023.114327

Chen H, Gao Y, Shu S and Lai Y (2023) The six-degree-of-freedom behavior of drag embedment anchor installed in clay. *Ships and Offshore Structures*, 19(4): 461–470. http://doi.org/10.1080/17445302.2023.2177029

Dao D, Grabe J, da Silva AP, Langstraat J, Su Y, Castelein K, de Lange D, Luger D and van Eekelen S (2025) Centrifuge modelling of anchor performance for floating offshore wind turbines: installation and load behaviour in sand. *Proceedings of the 5th International Symposium on Frontiers in Offshore Geotechnics (ISFOG 2025)*. http://doi.org/10.53243/ISFOG2025-122

Dao DA, Grabe J, Peccin da Silva A, Langstraat JHA, Su YY, Castelein K, de Lange DA, Luger D and van Eekelen SJ (2024) Geolab project: ISEDEA - influence of storm events on drag embedment anchor behaviour for floating offshore wind turbines. Dataset. http://doi.org/10.5281/zenodo.14552391

Davidson C, Brennan A, Brown M, Inglis L and Vasudevan S (2023) Out of plane loading of drag embedment anchors for floating renewable energy technologies. *Proceedings of the 9th International SUT OSIG Conference "Innovative Geotechnologies for Energy Transition"*, pp. 1241–1248. http://doi.org/10.3723/ZYHR1120

de Lange DA and Langstraat JHA (2024) A procedure to colour sand grains. *Proceedings of the 5th European Conference on Physical Modelling in Geotechnics*. http://doi.org/10.53243/ECPMG2024-85

Delmar (2018) Vryhof manual - the guide to anchoring.

Fan J, Ferrell B, O'Loughlin CD, Bransby MF and Watson PG (2026) Combined 6-DoF motion tracking and photogrammetry to capture drag anchor installation behaviour in sand. *Proceedings of the 11th International Conference on Physical Modelling in Geotechnics (ICPMG 2026).*

Gourvenec S (2024) Offshore geotechnical challenges of the energy transition. *Geomechanics for Energy and the Environment*, 39: 100584. http://doi.org/10.1016/j.gete.2024.100584

Hong S, McMorland J, Zhang H, Collu M and Halse KH (2024) Floating offshore wind farm installation, challenges and opportunities: A comprehensive survey. *Ocean Engineering*, 304: 117793. http://doi.org/10.1016/j.oceaneng.2024.117793

Jamiolkowski M., Lo Presti DCF and Manassero M (2003). Evaluation of relative density and shear strength of sands from CPT and DMT. *Soil Behavior and Soft Ground Construction*, 201–238. http://doi.org/10.1061/40659(2003)7

Lai Y, Zhu B, Huang Y and Chen C (2020) Behaviors of drag embedment anchor in layered clay profiles. *Applied Ocean Research*, 101: 102287. http://doi.org/10.1016/j.apor.2020.102287

Neubecker SR and Randolph MF (1996a) The kinematic behaviour of drag anchors in sand. *Canadian Geotechnical Journal*, 33(4): 584–594. https://doi.org/10.1139/t96-084-306

Neubecker SR and Randolph MF (1996b) The static equilibrium of drag anchors in sand. *Canadian Geotechnical Journal*, 33(4): 574–583. http://doi.org/10.1139/t96-083-305

O'Neill M and Randolph M (2001) Modelling drag anchors in a drum centrifuge. *International Journal of Physical Modelling in Geotechnics*, 1(2): 29–41, http://doi.org/10.1680/ijpmg.2001.010203

O'Neill MP, Bransby MF and Randolph MF (2003) Drag anchor fluke–soil interaction in clays. Canadian Geotechnical Journal 40(1): 78–94. http://doi.org/10.1139/t02-096

Randolph M and Gourvenec S (2017). Offshore geotechnical engineering. CRC press. http://doi.org/10.1201/9781315272474

Schulz CW, Wang K, Wieczorek K, Netzband S and Abdel-Maksoud M (2022) Experimental and numerical investigation of the yaw moment of a downwind coned wind turbine rotor. *Wind Energy*, 25(12): 1995–2015. http://doi.org/10.1002/we.2779

Sharif YU, Davidson C, Brown M, Brennan A, Coombs WM, Bird RE, Augarde C, Carter G, Macdonald C and Johnson KR (2025a) Centrifuge modelling of drag embedment anchors subjected to inclined loading for floating wind. *Proceedings of the 5th International Symposium on Frontiers in Offshore Geotechnics (ISFOG 2025).* http://doi.org/10.53243/ISFOG2025-627

Sharif YU, Brown M, Knappett J, Davidson C, Bird R, Coombs W, Augarde C, Carter G, Macdonald C and Johnson K (2025b). Comparison of 1 g and centrifuge modelling of drag anchors with subsurface wireless tracking. *International Journal of Physical Modelling in Geotechnics*, 25(2): 102–114. http://doi.org/10.1680/jphmg.24.00029